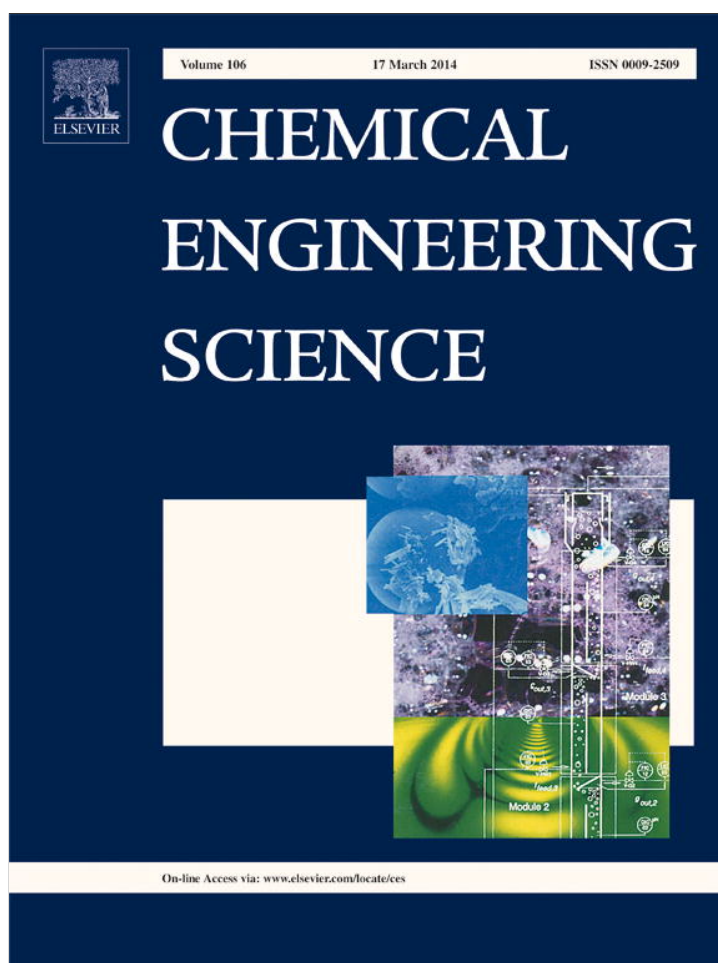


Provided for non-commercial research and education use.  
Not for reproduction, distribution or commercial use.



This article appeared in a journal published by Elsevier. The attached copy is furnished to the author for internal non-commercial research and education use, including for instruction at the authors institution and sharing with colleagues.

Other uses, including reproduction and distribution, or selling or licensing copies, or posting to personal, institutional or third party websites are prohibited.

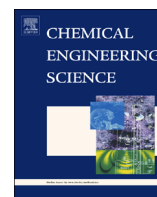
In most cases authors are permitted to post their version of the article (e.g. in Word or Tex form) to their personal website or institutional repository. Authors requiring further information regarding Elsevier's archiving and manuscript policies are encouraged to visit:

<http://www.elsevier.com/authorsrights>



Contents lists available at ScienceDirect

## Chemical Engineering Science

journal homepage: [www.elsevier.com/locate/ces](http://www.elsevier.com/locate/ces)

## Design tool and guidelines for outdoor photobioreactors

Euntaek Lee<sup>a</sup>, Jérémy Pruvost<sup>b</sup>, Xing He<sup>c</sup>, Ramakanth Munipalli<sup>c</sup>, Laurent Pilon<sup>a,\*</sup><sup>a</sup> Mechanical and Aerospace Engineering Department, Henry Samueli School of Engineering and Applied Science, University of California, 420 Westwood Plaza, Eng. IV 37-132, Los Angeles, CA 90095, USA<sup>b</sup> LUNAM Université, Université de Nantes, CNRS, GEPEA UMR 6144, Bd de l'Université, CRTT-BP 406, 44602 Saint-Nazaire Cedex, France<sup>c</sup> HyPerComp, Inc., 2629 Townsgate Rd., Suite 105, Westlake Village, CA 91361, USA

## AUTHOR HIGHLIGHTS

- Similarity behavior in biomass daily areal productivity of photobioreactors is demonstrated.
- It was valid for common PBRs in batch or continuous mode with various microorganisms.
- Productivity depended only on the ratio of initial concentration and illuminated area per unit volume.
- Results can be used as guidelines for outdoor photobioreactors design and operation.

## ARTICLE INFO

## Article history:

Received 22 June 2013

Received in revised form

17 October 2013

Accepted 10 November 2013

Available online 18 November 2013

## Keywords:

Photobiological hydrogen production

Biofuel

Design

Light transfer

Modeling

Optimization

## ABSTRACT

This study provides design and operational guidelines for achieving maximum biomass productivity in outdoor photobioreactors (PBRs). Detailed simulations of coupled light transfer and growth kinetics of microalgae were performed for open ponds, vertical flat-plate, and tubular PBRs operated in batch mode and exposed to time-dependent collimated and diffuse solar irradiance. The temporal evolution of microalgae concentration was predicted by accounting for light saturation, photoinhibition, and respiration. Three-dimensional spectral light transfer simulations of collimated and diffuse solar radiation in the PBRs were performed at different times of the day. The green microalgae *Chlamydomonas reinhardtii* was used for illustration purposes. The study demonstrated that the daily productivity per unit of illuminated surface area for PBRs operated in batch mode was identical and depended uniquely on the ratio  $X_0/a$  where  $X_0$  is the initial microalgae concentration and  $a$  is the illuminated surface area per unit volume of PBR. A maximum daily productivity of about 0.045 kg/m<sup>2</sup>/day was achieved for  $X_0/a = 0.035$  kg/m<sup>2</sup>. Remarkably, similar results were obtained with experimental data and other simulation results based on different models reported in the literature, for different microorganisms and PBRs operated in continuous mode. The PBR optical thickness, represented by  $X_0/a$ , constitutes a convenient parameter for designing (via  $a$ ) and operating (via  $X_0$ ) these PBRs to achieve their maximum performance.

© 2013 Elsevier Ltd. All rights reserved.

## 1. Introduction

Microalgae cultivation has received significant attention in recent years as a way to fixate CO<sub>2</sub> generated during fossil fuel combustion and to produce liquid or gaseous biofuels (Melis, 2002; Chisti, 2007) as well as food supplement (Skjånes et al., 2007) and protein for human or animal feed (Yoon et al., 2002). Photosynthetic microalgae use sunlight as their energy source, water as their electron source, and CO<sub>2</sub> as their carbon source. They are typically grown in open ponds and photobioreactors (PBRs) of various designs where sunlight is absorbed and scattered

by the microalgae kept in suspension by mechanical stirring and/or bubble sparging (Asenjo and Merchuk, 1995). To be economically viable, the processes require the highest microalgae productivity and efficiency. Open ponds or PBRs can be operated in batch or in continuous mode. Batch cultures are widely used for their simplicity, flexibility, and low cost (Barsanti and Gualtieri, 2005). Scaling-up benchtop PBRs to industrial scale remains a challenge (Morweiser et al., 2010). Indeed, optimum temperature, mixing, light, and mass transfer should be maintained in PBRs of any sizes (Ugwu et al., 2008). Current PBRs must be improved in order to achieve larger mass concentrations and growth rate and to minimize auxiliary energy use and capital cost (Posten, 2009).

The objective of this study is to develop accurate numerical simulation tools and to obtain design guidelines for the optimization and operation of efficient PBRs. To do so, light transfer in PBRs

\* Corresponding author. Tel.: +1 310 206 5598; fax: +1 310 206 2302.  
E-mail address: [pilon@seas.ucla.edu](mailto:pilon@seas.ucla.edu) (L. Pilon).

with various geometries exposed to solar radiation was analyzed on a spectral basis over the spectral region between 400 and 700 nm corresponding to the photosynthetically active radiation (PAR) region. The temporal evolution of microalgae concentration was also predicted using a growth kinetics model taking into account the local available light in the PBRs at different times of the day.

## 2. Background

### 2.1. Radiation transfer in photobioreactors

As light travels through the microalgae suspension contained in the PBR, it is absorbed by the microorganisms or by the medium and scattered by microorganisms and, possibly, by gas bubbles used to deliver CO<sub>2</sub> and to stir the suspension. Solar radiation intensity  $I_\lambda(\mathbf{r}, \hat{\mathbf{s}})$  at location  $\mathbf{r}$  traveling along direction  $\hat{\mathbf{s}}$  is governed by the radiative transfer equation (RTE) (Pilon et al., 2011).

The local spectral fluence rate, denoted by  $G_\lambda(\mathbf{r})$ , and the local fluence rate average over the PAR region between 400 and 700 nm, denoted by  $G_{PAR}(\mathbf{r})$ , available to microalgae at location  $\mathbf{r}$  are respectively defined as (Pilon et al., 2011),

$$G_\lambda(\mathbf{r}) = \int_{4\pi} I_\lambda(\mathbf{r}, \hat{\mathbf{s}}) d\Omega \quad \text{and} \quad G_{PAR}(\mathbf{r}) = \int_{400}^{700} G_\lambda(\mathbf{r}) d\lambda \quad (1)$$

The average fluence rate  $G_{av}$  over the entire PBR of volume  $V$  can be estimated from the local PAR-averaged fluence rate  $G_{PAR}(\mathbf{r})$  as

$$G_{av} = \frac{1}{V} \int_V G_{PAR}(\mathbf{r}) dV = \frac{1}{V} \int_V \left( \int_{400}^{700} G_\lambda(\mathbf{r}) d\lambda \right) dV \quad (2)$$

The two-flux approximation assumes one-dimensional radiation transfer and can account for in-scattering terms as well as anisotropic scattering (Modest, 2003). In cases when the PBR is exposed to both collimated and diffuse solar irradiances  $G_{in,c,\lambda}$  and  $G_{in,d,\lambda}$ , the total local spectral fluence rate  $G_\lambda(z)$  (in W/m<sup>2</sup>) can be estimated by summing up its collimated and diffuse components as (Pruvost et al., 2012)

$$G_\lambda(z) = G_{c,\lambda}(z) + G_{d,\lambda}(z) \quad (3)$$

Pottier et al. (2005) solved the RTE using the two-flux approximation to model light transfer in a one-dimensional flat-plate PBR with a transparent front window and a diffusely reflecting back side with spectral reflectance  $\rho_\lambda$ . The authors derived an analytical expression for the local spectral fluence rate  $G_{c,\lambda}(z)$  (in W/m<sup>2</sup>) in such PBRs exposed to solar irradiance  $G_{in,c,\lambda}$  incident onto the PBR at an angle  $\theta_c$  with respect to the surface's normal direction as (Pottier et al., 2005)

$$\frac{G_{c,\lambda}(z)}{G_{in,c,\lambda}} = 2 \sec \theta_c \frac{[\rho_\lambda(1+\alpha_\lambda)e^{-\delta_\lambda z} - (1-\alpha_\lambda)e^{-\delta_\lambda L}]e^{\delta_\lambda z} + [(1+\alpha_\lambda)e^{\delta_\lambda L} - \rho_\lambda(1-\alpha_\lambda)e^{\delta_\lambda L}]e^{-\delta_\lambda z}}{(1+\alpha_\lambda)^2 e^{\delta_\lambda L} - (1-\alpha_\lambda)^2 e^{-\delta_\lambda L} - \rho_\lambda(1-\alpha_\lambda^2)e^{\delta_\lambda L} + \rho_\lambda(1-\alpha_\lambda^2)e^{-\delta_\lambda L}} \quad (4)$$

where the parameters  $\alpha_\lambda$  and  $\delta_\lambda$  are expressed as (Pottier et al., 2005)

$$\alpha_\lambda = \sqrt{\frac{\bar{A}_{abs,\lambda}}{\bar{A}_{abs,\lambda} + 2b_\lambda \bar{S}_{sca,\lambda}}} \quad \text{and} \quad \delta_\lambda = X \sec \theta_c \sqrt{\bar{A}_{abs,\lambda}(\bar{A}_{abs,\lambda} + 2b_\lambda \bar{S}_{sca,\lambda})} \quad (5)$$

here  $\bar{A}_{abs,\lambda}$  and  $\bar{S}_{sca,\lambda}$  are the average mass absorption and scattering cross-sections (in m<sup>2</sup>/kg) while  $X$  is the microorganism mass concentration expressed in kg dry cell weight cells per m<sup>3</sup> of suspension (or kg/m<sup>3</sup>). The effective absorption and scattering coefficients of the suspension are given by

$$\kappa_\lambda = \bar{A}_{abs,\lambda} X \quad \text{and} \quad \sigma_{s,\lambda} = \bar{S}_{sca,\lambda} X \quad (6)$$

For an axisymmetric phase function, the backward scattering fraction, denoted by  $b_\lambda$ , is defined as (Pottier et al., 2005)

$$b_\lambda = \int_{\pi/2}^{\pi} \Phi_{T,\lambda}(\theta) \sin \theta d\theta \quad (7)$$

where  $\Phi_{T,\lambda}(\hat{\mathbf{s}}_i, \hat{\mathbf{s}})$  is the effective scattering phase function of the suspension. The local diffuse spectral fluence rate  $G_{d,\lambda}(z)$  can be estimated from Eqs. (4) and (5) by replacing  $\sec \theta_c$  by a factor 2.

### 2.2. Microalgae growth kinetics

The time rate of change of microalgae mass concentration  $X$  can be modeled as (Dunn et al., 2003)

$$\frac{dX}{dt} = \bar{\mu} X \quad (8)$$

where  $\bar{\mu}$  is the average total specific growth rate expressed in h<sup>-1</sup>. Various growth kinetics models have been developed to predict the local specific growth rate  $\mu$ . Fouchard et al. (2009) expressed the photosynthetic growth rate of *C. reinhardtii* as a function of local fluence rate  $G_{PAR}(\mathbf{r})$  at location  $\mathbf{r}$ , according to the Haldane model (Versyck et al., 1997), accounting for light limitation and photoinhibition as

$$\mu_p(\mathbf{r}) = \mu_0 \left( \frac{G_{PAR}(\mathbf{r})}{K_S + G_{PAR}(\mathbf{r}) + G_{PAR}^2(\mathbf{r})/K_I} \right) \quad (9)$$

where  $\mu_0$  is the so-called maximum specific growth rate while the coefficients  $K_S$  and  $K_I$  are the light half-saturation and inhibition constants, respectively. The authors also considered reduction in growth rate due to cellular respiration as the catabolic process. Then, the total local specific growth rate  $\mu(\mathbf{r})$  can be expressed as (Fouchard et al., 2009)

$$\mu(\mathbf{r}) = \mu_p(\mathbf{r}) - \mu_s \quad (10)$$

where  $\mu_s$  is the respiration rate assumed to be constant at all times and locations (Fouchard et al., 2009). In addition, the average total specific growth rate  $\bar{\mu}$  over the PBR volume can be estimated as (Fouchard et al., 2009)

$$\bar{\mu} = \frac{1}{V} \int_V \mu(\mathbf{r}) dV \quad (11)$$

### 2.3. Photobioreactor modeling

Modeling of PBR typically consists of solving the RTE coupled with a growth kinetics model. Aiba (1982) calculated the light intensity distribution and absorbance in one-dimensional flat-plate PBR with microalgae *Rhodospseudomonas spheroides* using the Monte Carlo method. The author considered anisotropic scattering and neglected reflection at the walls. He compared the absorbance obtained by the Monte Carlo method with that obtained by Beer–Lambert's law as a function of cell concentration. Beer–Lambert's law was found to overestimate the absorbance in the PBR because it does not consider in-scattering (Aiba, 1982). This was also illustrated by Berberoğlu et al. (2007a).

Cornet et al. (1992), Cornet and Albiol (2000), and Cornet and Dussap (2009) developed a coupled light transfer and Haldane growth kinetics model to estimate the biomass volumetric production rate of one-dimensional flat-plate PBRs. The local fluence rate was estimated using the two-flux approximation. They introduced the concept of working illuminated volume which, combined with their models, can be used to retrieve the growth kinetic parameters. Based on this approach Fouchard et al. (2009) retrieved the growth kinetics parameters of *C. reinhardtii* cultivated in a torus PBR with continuous injection of N<sub>2</sub> and CO<sub>2</sub> gases

and illuminated with white light from fluorescent tubes considering biomass concentration, extracellular sulfur concentration, and intracellular quota. Finally, these models have been validated experimentally for different (i) PBR shapes and volumes, (ii) incident irradiance, (iii) microorganism species, and (iv) carbon sources.

Wheaton and Krishnamoorthy (2012) simulated light transfer coupled with fluid hydrodynamics within an air-lift tubular PBR illuminated from inside by fluorescent lamps. The authors identified the effects of angular discretization, scattering phase function, air mass flow rate, and bubble size on the local fluence rate. They used the finite volume method to solve the 3D RTE based on spectrally averaged incident radiation and radiation characteristics of cyanobacterium *Synechococcus* sp. over three spectral bands in the PAR region. They concluded that scattering by bubbles resulted in redistribution of the light but was negligible at high microalgae concentrations, as previously reported (Berberoğlu et al., 2007b).

Murphy and Berberoğlu (2011) coupled light transfer with a photosynthetic rate model for *C. reinhardtii* wild strain and transformant *tla1* within plane parallel PBR considering photo-inhibition. The authors solved the one-dimensional RTE using the discrete ordinates method to estimate the local fluence rate. They calculated the local specific and total oxygen production as a function of optical thickness for different incident irradiances.

Slegers et al. (2011) simulated outdoor vertical flat-plate PBRs operated in continuous mode and containing *Phaeodactylum tricornutum* or *Thalassiosira pseudonana*. The authors coupled light transfer with a growth kinetics model to estimate volumetric daily and yearly biomass productivity. They treated the suspensions as gray with constant radiation characteristics averaged over the PAR region and used Beer–Lambert's law to calculate the average fluence rate within the PBR and a growth kinetic model based on *pI*-curves accounting for respiration (Geider et al., 1996). They also defined the average total specific growth rate based on Eq. (11). They investigated the effect of thickness and biomass concentration on the volumetric productivity of PBRs in the Netherlands.

Huang et al. (2012) simulated annular PBR with *Porphyridium cruentum* in continuous and batch cultures. The authors integrated hydrodynamics, radiation transfer, and growth kinetics models to predict biomass concentration as a function of time. The 3D RTE was solved using the finite volume method and the discrete ordinate method to estimate the light intensity within the annular PBR. The box model with two boxes was used to account for spectral radiation in normal diffuse incident irradiance and radiation characteristics of microalgae to estimate the light intensity within the annular PBR. Good agreement was observed between the numerical prediction of biomass concentration and the experimental data reported in the literature (Muller-Feuga et al., 2003).

Finally, Pruvost et al. (2012) simulated outdoor inclined rectangular PBR exposed to solar irradiance with cyanobacterium *Arthrospira platensis* grown in continuous culture. The authors coupled light transfer with the growth kinetics model to estimate the biomass productivity per unit surface area illuminated. They calculated the fluence rate using the two-flux approximation for constant biomass concentration. They investigated the effects of latitude and inclination of the PBR surface on the maximum areal biomass productivity. The location close to Earth's equator had biomass productivity up to 40% larger than those at higher latitudes. In addition, the areal biomass productivity achieved with a solar tracking system was 30% larger than that obtained with constant inclination.

Previous studies often used spectrally averaged incident irradiance and radiation characteristics. In addition, light transfer in PBRs has frequently been treated as one-dimensional and estimated using either Beer–Lambert's law or the two-flux approximation. Most studies also considered constant and normally collimated incident irradiance. However, solar irradiance fluctuates in direction and

intensity during the day. Also, radiation characteristics of microalgae depend strongly on wavelength. In addition, actual PBRs may have complex geometries for which simplified radiation model may not be valid.

Moreover, Richmond (1996), Richmond and Qiang (1997) and Richmond (2004) suggested the need for a unifying approach to PBR design and operation and emphasized the connection between light intensity, cell density, and the optical thickness of the PBR to maximize microalgal productivity. The authors demonstrated the need to optimize these parameters for a given microalgae species and provided qualitative guidelines obtained from experimental studies. In particular, they recommended ultra-high

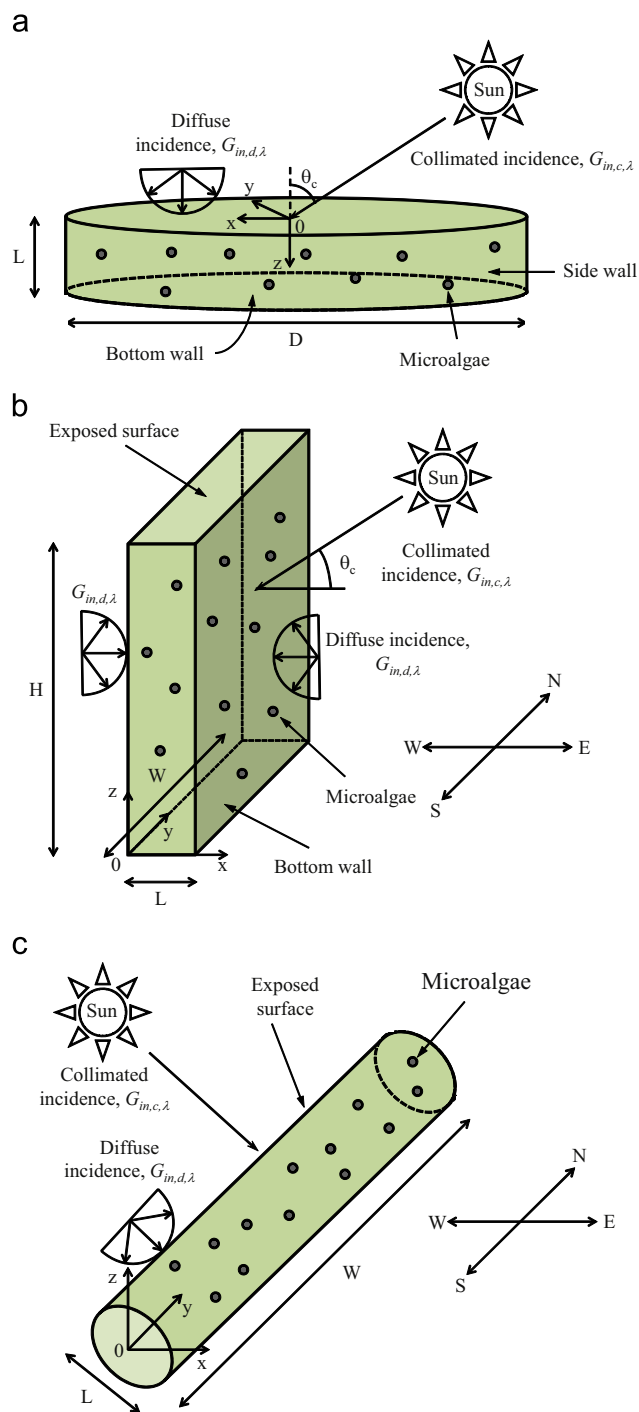


Fig. 1. Schematic of the (a) open pond, (b) vertical flat-plate, and (c) tubular photobioreactors simulated in this study along with coordinate systems.

cell density cultures in PBRs with short path length to achieve efficient utilization of solar radiation. Under these conditions, they also discussed the importance of turbulent mixing to increase the light/dark cycle frequency. However, quantitative criteria for optimum productivity were not provided.

In this study, light transfer was accurately simulated by solving the three-dimensional RTE on a spectral basis using experimentally measured spectral radiation characteristics of *C. reinhardtii* (Berberoğlu et al., 2008). Both spectral diffuse and collimated solar irradiances with different incident angles corresponding to different times of the day were considered. It was coupled with the Haldane growth kinetics model accounting for photolimitation, photoinhibition, and cellular respiration. The fluence rate, biomass concentration, and daily productivity of outdoor open ponds, vertical flat-plate, and tubular PBRs were compared and discussed with experimental and numerical results reported in the literature. Quantitative criteria to achieve maximum productivity were also derived in terms of cell density and PBR dimensions for a given microalgae species.

### 3. Methods

#### 3.1. Problem statement

Algal biomass production in PBRs depends on numerous parameters including (i) the cultivation location, (ii) the day of the year and the time of the day along with (iii) the corresponding solar irradiance, (iv) the microalgae species, (v) the initial mass concentration, (vi) the PBR geometry, and (vii) its wall reflection and refraction. The present study simulates light transfer and microalgae growth in common PBRs located in Los Angeles, CA, USA (34.04°N, 118.15°W). Simulations were performed for circular open pond, single standing vertical flat-plate, and horizontal tubular PBRs. The PBRs were aligned along the north–south direction and exposed to solar irradiance comprised both a collimated and a diffuse component. Note that in all cases, we ignored shading by other PBR systems. In other words, ideal situations were considered to fairly compare the three different PBR geometries considered. Fig. 1 shows the geometries, dimensions, and boundary conditions of the PBRs simulated in this study along with the associated coordinate systems. The open pond had depth  $L$  varying from 0.05 to 1.0 m. The thickness  $L$  of the vertical flat-plate PBR ranged from 0.05 to 1.0 m while the diameter  $L$  of the tubular PBR varied from 0.1 to 1.0 m. *C. reinhardtii* were simulated for illustration purposes and because its growth kinetic parameters were known (Fouchard et al., 2009).

#### 3.2. Assumptions

In order to predict light transfer and the temporal evolution of microalgae concentration in the different PBRs considered, it was assumed that (1) the microalgae were well mixed, randomly oriented, and uniformly distributed in the PBR. In practice, this is achieved by stirring the PBR with paddle wheels or gas sparging, for example. (2) The liquid medium was non-emitting (cold) and non-scattering over the PAR region. (3) The absorption coefficient of the medium was the same as that of water. (4) The radiation characteristics of *C. reinhardtii* remained the same throughout the day. (5) Bubbles potentially used for stirring purposes featured interfacial area concentration smaller than  $450 \text{ m}^{-1}$  so their effect on light transfer could be neglected (Berberoğlu et al., 2007b). (6) The PBR was neither mass transfer nor nutrient limited and operated at constant temperature. (7) The photosynthetic specific growth rate  $\mu_p$  was only a function of the local and average fluence rate available in the PBRs and given by Eq. (9). (8) Finally, biomass

loss at night due to respiration was ignored as PBR productivity was estimated after 12 h of exposure to sunlight. For longer duration (succession of day–night cycles), losses to the respiration at night must be considered (Le Borgne and Pruvost, 2013).

#### 3.3. Governing equations

The radiation intensity  $I_\lambda(\mathbf{r}, \hat{\mathbf{s}})$  in direction  $\hat{\mathbf{s}}$  at location  $\mathbf{r}$  can be decomposed as the sum of a collimated  $I_{c,\lambda}(\mathbf{r}, \hat{\mathbf{s}})$  and a diffuse  $I_{d,\lambda}(\mathbf{r}, \hat{\mathbf{s}})$  component so that (Modest, 2003)

$$I_\lambda(\mathbf{r}, \hat{\mathbf{s}}) = I_{c,\lambda}(\mathbf{r}, \hat{\mathbf{s}}) + I_{d,\lambda}(\mathbf{r}, \hat{\mathbf{s}}) \quad (12)$$

The steady-state RTE for the collimated intensity can be written as

$$\hat{\mathbf{s}} \cdot \nabla I_{c,\lambda}(\mathbf{r}, \hat{\mathbf{s}}) = -\kappa_\lambda I_{c,\lambda}(\mathbf{r}, \hat{\mathbf{s}}) - \sigma_{s,\lambda} I_{c,\lambda}(\mathbf{r}, \hat{\mathbf{s}}) \quad (13)$$

This first and second terms on the right-hand-side of Eq. (13) account for the fact that the collimated incident radiation along the collimated direction decays as it travels through the microalgae suspension due to absorption and scattering, respectively. Similarly, the steady-state RTE for the diffuse intensity  $I_{d,\lambda}(\mathbf{r}, \hat{\mathbf{s}})$  can be written as (Modest, 2003)

$$\hat{\mathbf{s}} \cdot \nabla I_{d,\lambda}(\mathbf{r}, \hat{\mathbf{s}}) = -\kappa_\lambda I_{d,\lambda}(\mathbf{r}, \hat{\mathbf{s}}) - \sigma_{s,\lambda} I_{d,\lambda}(\mathbf{r}, \hat{\mathbf{s}}) + \frac{\sigma_{s,\lambda}}{4\pi} \int_{4\pi} I_{d,\lambda}(\mathbf{r}, \hat{\mathbf{s}}_i) \Phi_\lambda(\hat{\mathbf{s}}_i, \hat{\mathbf{s}}) d\Omega_i + \frac{\sigma_{s,\lambda}}{4\pi} \int_{4\pi} I_{c,\lambda}(\mathbf{r}, \hat{\mathbf{s}}_i) \Phi_\lambda(\hat{\mathbf{s}}_i, \hat{\mathbf{s}}) d\Omega_i \quad (14)$$

The last two terms of Eq. (14) account for multiple scattering of the diffuse and collimated radiation intensities. In fact, the diffuse incident radiation along direction  $\hat{\mathbf{s}}$  at location  $\mathbf{r}$  is not only absorbed and scattered but also reinforced as diffuse and collimated radiations from any direction  $\hat{\mathbf{s}}_i$  over  $4\pi$  solid angle get scattered in direction  $\hat{\mathbf{s}}$ .

#### 3.4. Radiation characteristics of *C. reinhardtii*

The effective absorption coefficient  $\kappa_\lambda$  of the suspension can be expressed in terms of the microorganism mass concentration  $X$  as (Berberoğlu and Pilon, 2010)

$$\kappa_\lambda = \kappa_{L,\lambda}(1 - \nu X) + \bar{A}_{abs,\lambda} X \quad (15)$$

where  $\nu$  is the specific volume of microorganisms assumed to be equal to  $0.001 \text{ m}^3/\text{kg}$ . The absorption coefficient of the liquid phase  $\kappa_{L,\lambda}$  is expressed in  $\text{m}^{-1}$  and given by (Modest, 2003)

$$\kappa_{L,\lambda} = \frac{4\pi k_\lambda}{\lambda} \quad (16)$$

where  $k_\lambda$  was taken as the absorption index of water reported by Hale and Querry (1973). On the other hand, the effective scattering coefficient  $\sigma_{s,\lambda}$  of the suspension can be expressed as (Berberoğlu and Pilon, 2007)

$$\sigma_{s,\lambda} = \bar{S}_{sca,\lambda} X \quad (17)$$

The average mass absorption and scattering cross-sections  $\bar{A}_{abs,\lambda}$  and  $\bar{S}_{sca,\lambda}$  along with the Henyey–Greenstein asymmetry factor of *C. reinhardtii* between 400 and 750 nm were reported in the literature (Berberoğlu et al., 2008). Alternatively, they could have been predicted by Lorenz–Mie theory using the complex index of refraction retrieved by Lee et al. (2013).

#### 3.5. Boundary and initial conditions

The solar spectrum incident on Earth depends on the latitude, longitude, and altitude. In this study, the Simple Model of the Atmospheric Radiative Transfer of Sunshine (SMARTS) (Gueymard, 2002) was used to predict the incident collimated and diffuse solar irradiances at sea level in Los Angeles, CA on June 21 at different times of the day. Fig. 2 shows the incident (a) collimated and

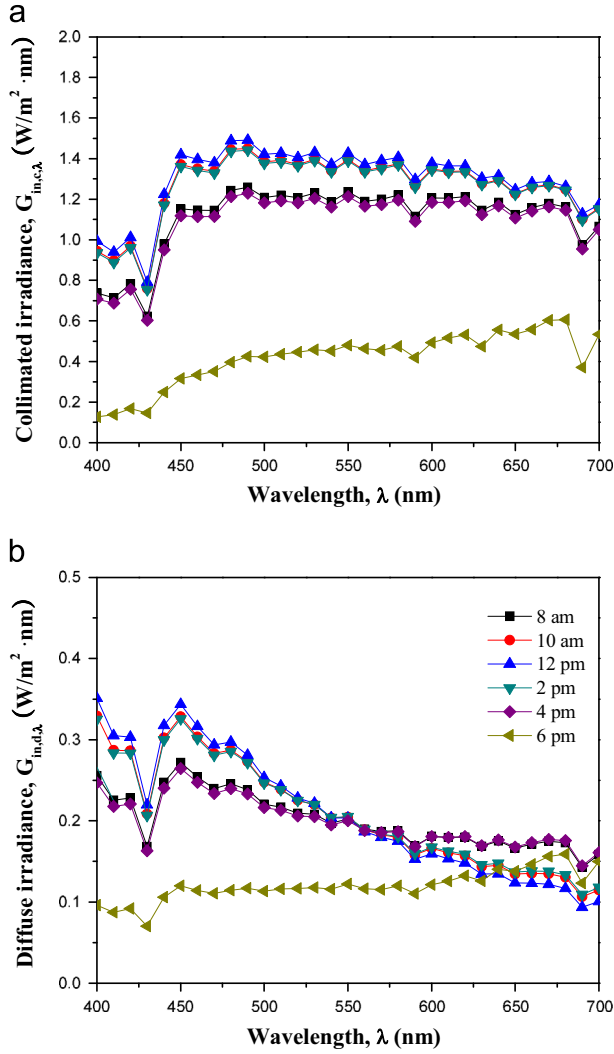


Fig. 2. Incident (a) collimated  $G_{in,c,\lambda}$  and (b) diffuse  $G_{in,d,\lambda}$  solar irradiance spectrum over the PAR region at different times of the day.

(b) diffuse solar irradiances respectively denoted by  $G_{in,c,\lambda}$  and  $G_{in,d,\lambda}$  in the PAR region at different times of the day on June 21 in Los Angeles. These irradiances were used in the boundary conditions necessary to solve Eqs. (13) and (14) according to  $I_{c,\lambda}(\mathbf{r}_{wall}, \hat{\mathbf{s}}) = G_{in,c,\lambda}$  and  $I_{d,\lambda}(\mathbf{r}_{wall}, \hat{\mathbf{s}}) = G_{in,d,\lambda}/2\pi$ , respectively. Here, the denominator  $2\pi$  corresponds to the solid angle of the hemisphere through which the diffuse irradiance  $G_{in,d,\lambda}$  is incident on the PBR (Modest, 2003).

The other boundary conditions depend on the PBR geometry. The open ponds were assumed to have transparent top surface, i.e., reflection by the air–water interface was neglected since it does not exceed 6% over the PAR region for incident angle within 60° of the normal to the pond surface according to Fresnel's law (Modest, 2003). Note that the pond surface is strongly reflecting at glazing incident angles corresponding to sunrise and sunset. Then, however, the intensity incident on the PBR was insufficient to significantly affect the biomass concentration. In addition, the bottom and side walls of the pond were treated as black ( $\rho_\lambda = 0$ ) or diffusely reflecting ( $\rho_\lambda = 1$ ). Refraction by the panels of the vertical flat-plate PBRs with constant index of refraction of 1.49 over the PAR region was also considered. The results were compared with those of simulations treating the PBR walls as transparent. Based on result from the flat-plate PBRs, the wall of the tubular PBRs was assumed to be transparent and refraction by the tube wall was ignored, as discussed in Sections 4.2 and 4.3.

### 3.6. Two-flux approximation

The analytical expression derived by Cornet et al. (1992) for predicting the local fluence rate  $G_\lambda(z)$  in vertical flat-plate PBRs exposed to collimated solar irradiance with reflecting back wall [Eq. (4)] can be extended to vertical flat-plate PBRs with transparent faces, one exposed to direct collimated and diffuse incident solar irradiance  $G_{in,c,\lambda}$  and  $G_{in,d,\lambda}$  and the other exposed only to diffuse solar irradiance  $G_{in,d,\lambda}$ . Then, the local spectral fluence rate at time  $t$  can be expressed as

$$G_\lambda(z, t) = G_{in,c,\lambda}(t)f_c(z) + G_{in,d,\lambda}(t)f_d(z) + G_{in,d,\lambda}(t)f_d(L-z) \quad (18)$$

where  $f_c(z)$  is defined as

$$f_c(z) = 2 \sec \theta_c(t) \frac{(1 + \alpha_\lambda) e^{\delta_\lambda L} e^{-\delta_\lambda z} - (1 - \alpha_\lambda) e^{-\delta_\lambda L} e^{\delta_\lambda z}}{(1 + \alpha_\lambda)^2 e^{\delta_\lambda L} - (1 - \alpha_\lambda)^2 e^{-\delta_\lambda L}} \quad (19)$$

and  $f_d(z)$  is expressed as

$$f_d(z) = 4 \frac{(1 + \alpha_\lambda) e^{\delta_{d,\lambda} L} e^{-\delta_{d,\lambda} z} - (1 - \alpha_\lambda) e^{-\delta_{d,\lambda} L} e^{\delta_{d,\lambda} z}}{(1 + \alpha_\lambda)^2 e^{\delta_{d,\lambda} L} - (1 - \alpha_\lambda)^2 e^{-\delta_{d,\lambda} L}} \quad (20)$$

here  $\alpha_\lambda$  and  $\delta_\lambda$  are given by Eq. (5) while

$$\delta_{d,\lambda} = 2X \sqrt{A_{abs,\lambda}(\bar{A}_{abs,\lambda} + 2b_\lambda \bar{S}_{sca,\lambda})}$$

Moreover, Berberoğlu et al. (2008) reported that the Henyey–Greenstein asymmetry factor of *C. reinhardtii* was 0.98 corresponding to strongly forward scattering, typical of microalgae. Then, the backward scattering fraction  $b_\lambda$  given by Eq. (7) can be assumed to be zero and  $\alpha_\lambda \approx 1$ . Then, the fluence rate in vertical flat-plate PBR exposed to collimated and diffuse incident radiation simplifies to

$$G_\lambda(z, t) = \sec \theta_c(t) G_{in,c,\lambda}(t) e^{-\delta_\lambda z} + 2G_{in,d,\lambda}(t) [e^{-\delta_{d,\lambda} z} + e^{-\delta_{d,\lambda}(L-z)}] \quad (21)$$

where  $\delta_\lambda$  and  $\delta_{d,\lambda}$  simplify to  $\delta_\lambda = \bar{A}_{abs,\lambda} X(t) \sec \theta_c(t)$  and  $\delta_{d,\lambda} = 2\bar{A}_{abs,\lambda} X(t)$ . Similarly, the fluence rate in open ponds with reflecting back wall can be expressed as

$$G_\lambda(z, t) = G_{in,c,\lambda}(t)f_c(z) + G_{in,d,\lambda}(t)f_d(z) \quad (22)$$

If  $\alpha_\lambda \approx 1$ , the two-flux approximation for open-ponds simplifies to

$$G_\lambda(z, t) = [G_{in,c,\lambda}(t) \sec \theta_c(t) + 2G_{in,d,\lambda}(t)] [e^{-\delta_\lambda z} + \rho_\lambda e^{-\delta_\lambda(2L-z)}] \quad (23)$$

These expressions apply also in the case of open ponds with black walls with  $\rho_\lambda = 0$ .

### 3.7. Method of solution

#### 3.7.1. Light transfer

The 3D RTE given by Eqs. (13) and (14) was solved numerically for  $I_\lambda(\mathbf{r}, \hat{\mathbf{s}})$  using the discontinuous Galerkin method. A detailed description of the DG method used in the present study and its validation was presented by He et al. (2013) and need not be repeated. Sunlight incident on the PBRs consists of a collimated and a diffuse component. The direction  $\theta_c(t)$  of collimated incidence changed during the course of the day. Unfortunately, conventional angular discretization methods such as discrete ordinate  $S_N$  (Fiveland and Wessel, 1988) and  $T_N$  (Chui and Raithby, 1993) approximations typically use fixed discrete directions. Therefore, the discretization would need to be changed for simulating different hours of the day (Li et al., 2004). A discrete ordinate scheme with infinitely small weight (DOS+ISW) (Li et al., 2004) was employed in this study to simulate collimated sunlight incident on the PBRs during the course of the day. It consists of adding a discrete direction, corresponding to the direction of collimated irradiance, directly to a conventional discrete ordinate quadrature. The weight associated with this new discrete direction is set to be infinitely small (Li et al., 2004). Thus, the new discrete direction has no effect on the zeroth-, first-, and second-order moments of the intensity (Li et al., 2004).

Finally, unstructured tetrahedral elements were employed for spatial discretization. The number of elements varied depending on the size of the PBRs. The  $S_4$  angular discretization, consisting of 6 discrete ordinate directions per quadrant, was used. The PAR region, defined from 400 to 700 nm, was discretized in 10 nm increments for a total of 31 wavelengths. To obtain a numerically converged solution of the RTE, the P-3 DG method was used in all simulations with a maximum number of elements in simulating open ponds, vertical flat-plate, and tubular PBRs equal to 95,633, 91,257, and 112,464, respectively.

### 3.7.2. Growth kinetics

In the present study, the growth kinetics model described by Eqs. (8)–(11) was used to determine the temporal evolution of microalgae concentration in PBRs. Fouchard et al. (2009) measured the average specific growth rate  $\bar{\mu}$  of the green algae *C. reinhardtii*. The authors estimated the parameters  $\mu_0$ ,  $\mu_s$ ,  $K_S$ , and  $K_I$  of the Haldane model to be  $0.2274 \text{ h}^{-1}$ ,  $0.032 \text{ h}^{-1}$ ,  $81.38 \text{ } \mu\text{mol photon m}^{-2} \text{ s}^{-1}$ , and  $2500 \text{ } \mu\text{mol photon m}^{-2} \text{ s}^{-1}$ , respectively for local irradiance  $G_{\text{PAR}}(\mathbf{r})$  ranging from 0 to  $400 \text{ } \mu\text{mol photon m}^{-2} \text{ s}^{-1}$ . These parameters resulted in prediction for  $\mu$  in good agreement with experimental data reported by Janssen et al. (2000). They were used in the present study after converting  $K_S$  and  $K_I$ , expressed in  $\mu\text{mol photon m}^{-2} \text{ s}^{-1}$ , in  $\text{W/m}^2$  using the conversion factor,  $1 \text{ } \mu\text{mol photon m}^{-2} \text{ s}^{-1} \approx 0.2174 \text{ W/m}^2$  over the PAR region (Morel and Smith, 1974).

### 3.7.3. Solution procedure

The mass concentration of microalgae as a function of time was obtained by the following procedure. First, the initial mass concentration of microalgae was set as  $X(t=0)=X_0$  at initial time 8:00 am. The corresponding effective absorption coefficient  $\kappa_\lambda$  and the scattering coefficient  $\sigma_{s,\lambda}$  were estimated using Eqs. (15) and (17), respectively. Then, Eqs. (13) and (14) were solved for  $I_{\lambda,c}$  and for  $I_{\lambda,d}$  using the DG method. Then, the local fluence rate

was estimated using Eq. (1). The corresponding local photosynthetic specific growth rate  $\mu_p$  was estimated [Eq. (9)] and used to calculate the average total specific growth rate  $\bar{\mu}$  [Eq. (11)] and the microalgae mass concentration  $X(t)$  [Eq. (8)] at subsequent time. This procedure was repeated by an increment of 2 h. During that time interval, the local fluence rate and average total specific growth rate were assumed to be constant. To ensure that numerical convergence had been reached with a time increment of 2 h, the temporal evolution of the biomass concentration  $X(t)$  in open ponds was predicted for 12 h with initial mass concentration  $X_0=0.1 \text{ kg/m}^3$  using the two-flux approximation and the above growth kinetics model. The local fluence rate obtained for time intervals of 30 min, 1 h, and 2 h were compared at 8:00 am, 10:00 am, 12:00 pm (noon), 2:00 pm, 4:00 pm, and 8:00 pm (see Supplementary Material). The maximum relative errors in the corresponding  $\bar{\mu}(t)$  and  $X(t)$  throughout the day were less than 3% and 6%, respectively. Thus, a 2 h time increment was judged to be a good compromise between accuracy and computing time for simulating coupled radiation transfer and microalgae growth kinetics in the PBR throughout the day.

## 4. Results and discussion

### 4.1. Open ponds

Fig. 3 shows the local PAR-averaged fluence rate  $G_{\text{PAR}}(\mathbf{r})$  in the east/west center plane of the circular open pond with either (a) black or (b) reflecting side and bottom walls at times 8:00 am, 10:00 am, 12:00 pm (noon), 2:00 pm, and 4:00 pm. Here, the pond diameter  $D$ , depth  $L$ , and initial mass concentration  $X_0$  were taken as 2 m, 0.1 m, and  $0.1 \text{ kg/m}^3$ , respectively. By comparing Figs. 3a and 3b, it is evident that the reflecting walls increased the local fluence rate in the PBR, particularly before 4:00 pm. However, the relative difference, in terms of mass concentration  $X(t)$ , between open ponds with black and reflecting walls was less than

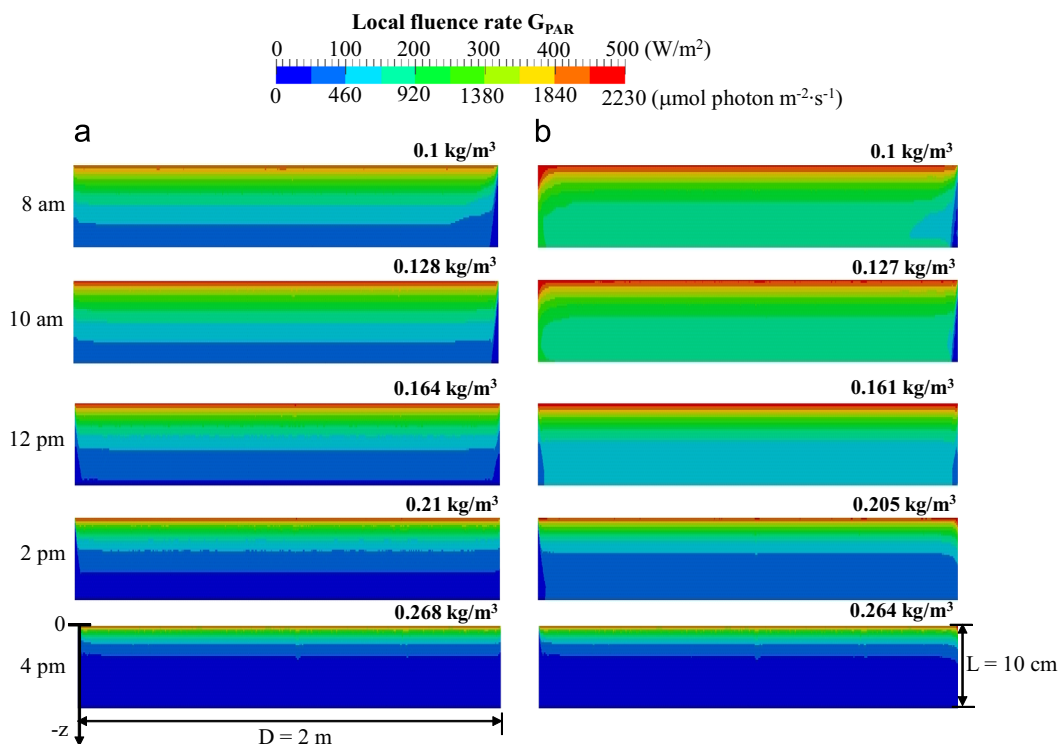


**Fig. 3.** Computed PAR-averaged local fluence rate  $G_{\text{PAR}}(\mathbf{r})$  on June 21, in Los Angeles at 8:00 am, 10:00 am, 12:00 pm, 2:00 pm, and 4:00 pm in the midplane of an open pond having diameter  $D=2 \text{ m}$  and depth  $L=0.1 \text{ m}$  with (a) black walls or (b) reflecting walls for initial mass concentration  $X_0=0.1 \text{ kg/m}^3$ .

1% after a day of growth. In both cases, the local fluence rate was nearly one-dimensional except near the side walls where shadows were apparent in the early morning and late afternoon. Note that even though, on June 21 in Los Angeles, the sun rises at 5:42 am and sets at 8:08 pm, the average total specific growth rate  $\bar{\mu}$  at times earlier than 8:00 am and later than 6:00 pm was less than  $0.01 \text{ h}^{-1}$  and growth was negligible.

#### 4.2. Vertical flat-plate photobioreactor

Light transfer in a vertical flat-plate PBR oriented north–south with initial mass concentration  $X_0=0.1 \text{ kg/m}^3$  was simulated over 12 h. The vertical flat-plate PBR height  $H$ , width  $W$ , and thickness  $L$  were taken as 2 m, 2 m, and 0.1 m, respectively. The walls were made of 8 mm thick glass panels. The effect of refraction due to mismatch in refractive indices of the air ( $n=1.0$ ), the reactor walls ( $n=1.49$ ), and the *C. reinhardtii* suspension ( $n=1.33$ ) contained in the PBR was investigated. These refraction indices were assumed to be constant over the PAR region. Reflection and refraction were estimated using Fresnel's equations for optically smooth and specularly reflecting surfaces (Modest, 2003).

Fig. 4 shows the local PAR-averaged fluence rate  $G_{PAR}(\mathbf{r})$  along a vertical cross-section of a 0.1 m thick flat-plate PBR accounting for refraction, at 8:00 am, 10:00 am, 12:00 pm (noon), 2:00 pm, 4:00 pm, and 6:00 pm. Three-dimensional effects were apparent between 10:00 am and 2:00 pm when the sun was near its zenith. During this time, the flat-plate PBR intercepted a small amount of collimated solar radiation. Sunlight was also incident on the PBR vertical windows at glazing angles when reflectance is large. Overall, accounting for refraction reduced slightly the local fluence rate compared with results obtained assuming the PBR wall to be transparent. The relative difference in *C. reinhardtii* mass concentration after 12 h was less than

0.1% when considering or ignoring refraction. Therefore, refraction of sunlight by the front and back windows of the PBR had negligible effects on the mass concentration of microalgae and could be ignored in our simulations.

#### 4.3. Tubular photobioreactor

A horizontal tubular PBR oriented in the north–south direction with initial mass concentration  $X_0=0.1 \text{ kg/m}^3$  was simulated over 12 h on June 21. Here, the tubular PBR diameter  $L$  was taken as 0.1 m. Fig. 5 shows the local PAR-averaged fluence rate  $G_{PAR}(\mathbf{r})$  over the cross-section of the pipe at different times of the day. It shows significant multidimensional effects. A darker region developed in the center of the tubular PBR under the combined effects of microalgae growth and the setting of the sun. Given the inherent 2D nature of this type of PBRs, the two-flux approximation could not be used.

#### 4.4. Two-flux approximation

Fig. 6a compares the local PAR-averaged fluence rate  $G_{PAR}(z)$  at the centerline of the open pond with black walls at times 8:00 am, 12:00 pm (noon), and 4:00 pm. It also compares the numerical predictions obtained using the DG method with predictions by the two-flux approximation [Eq. (22)] and by the simplified two-flux approximation [Eq. (23)]. The average relative difference between the numerical predictions using the DG method with DOS-ISW and the two-flux approximation for  $G_{PAR}(z)$  at the centerline of the open pond ranged between 4% and 10% depending on the time of the day and the location inside the PBR. However, prediction by the two-flux approximation was not able to predict the shadow and other multidimensional effects in the open pond. Moreover,

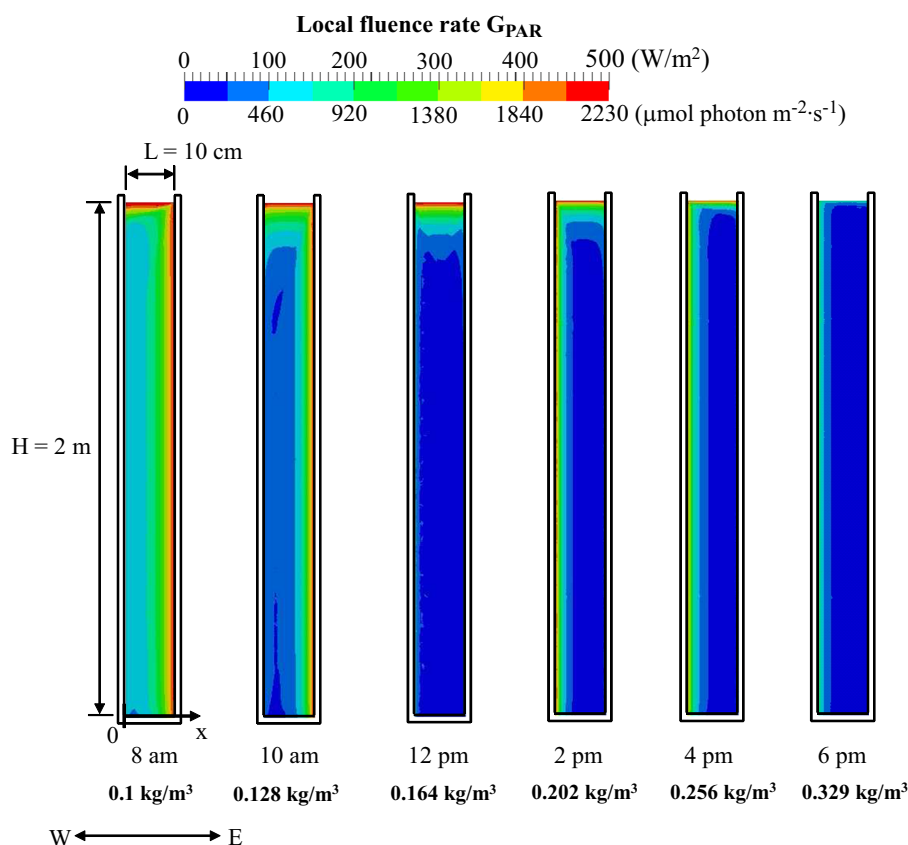


Fig. 4. Computed PAR-averaged local fluence rate  $G_{PAR}(\mathbf{r})$  on June 21 in Los Angeles at 8:00 am, 10:00 am, 12:00 pm, 2:00 pm, 4:00 pm, and 6:00 pm with refraction by the walls in the midplane of a single standing vertical flat-plate having height  $H=2$  m, width  $W=2$  m, and thickness  $L=0.1$  m with initial mass concentration  $X_0=0.1 \text{ kg/m}^3$ .

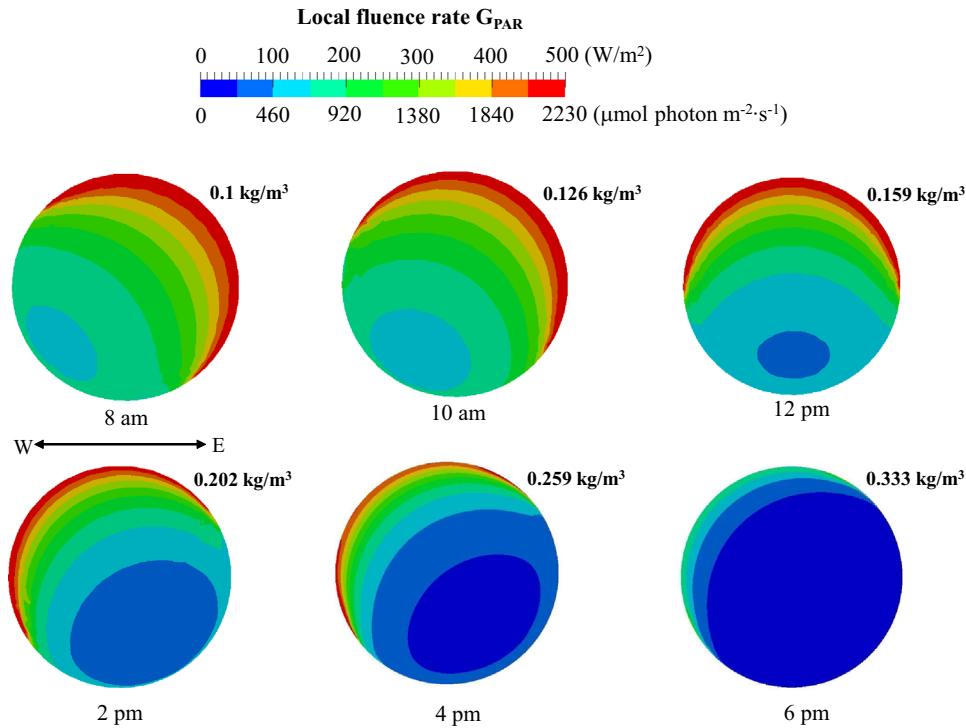


Fig. 5. Computed local PAR-averaged fluence rate  $G_{PAR}(\mathbf{r})$  on June 21 in Los Angeles at 8:00 am, 10:00 am, 12:00 pm, 2:00 pm, 4:00 pm, and 6:00 pm in the cross-section of north–south oriented single standing horizontal tubular PBRs having diameter  $L=0.1$  m with initial mass concentration  $X_0=0.1$  kg/m<sup>3</sup>.

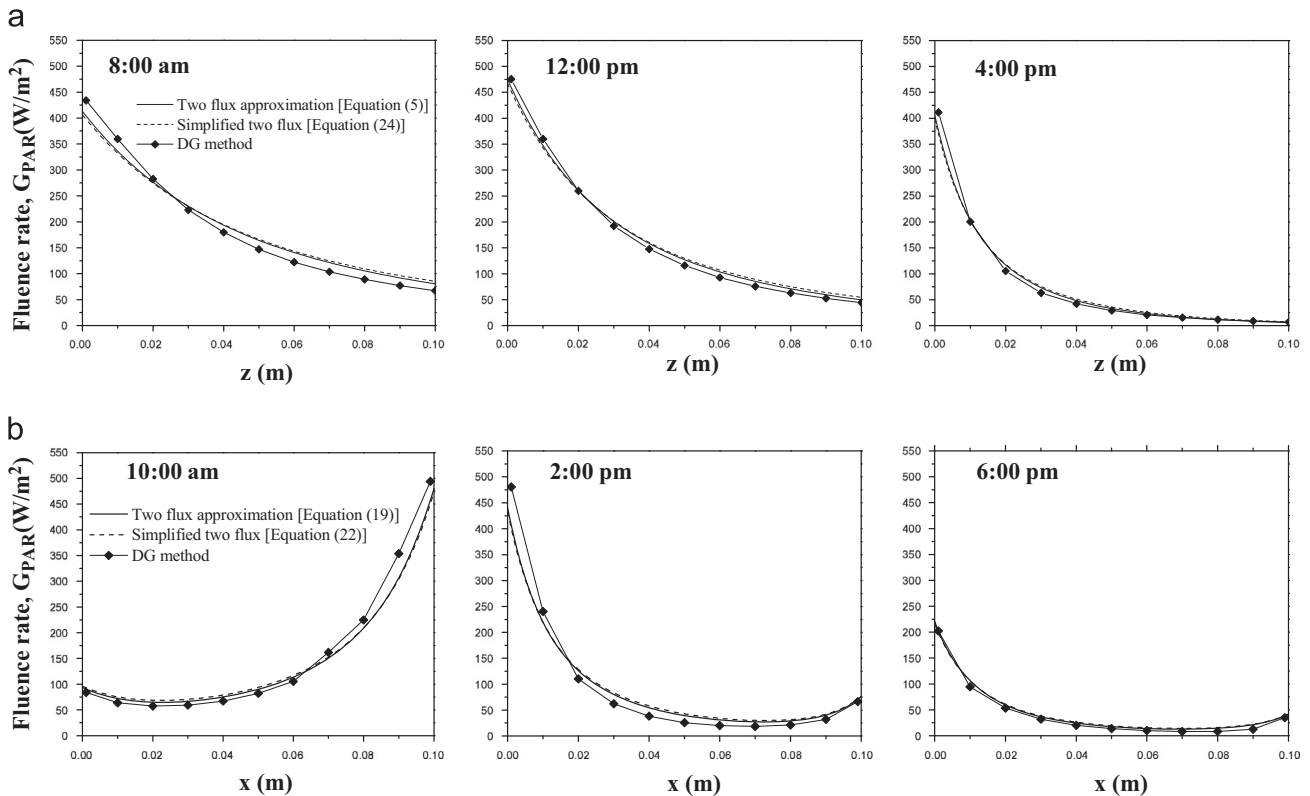


Fig. 6. PAR-averaged local fluence rate  $G_{PAR}(\mathbf{r})$  predicted on June 21 in Los Angeles (a) at 8:00 am, 12:00 pm, and 4:00 pm in the centerline of an open pond and (b) at 10:00 am, 2:00 pm, and 6:00 pm across a vertical flat plate PBR by (i) DG method with DOS-ISW, (ii) two-flux approximation [Eq. (4)], and (iii) simplified two-flux approximation [Eq. (23)]. The pond featured black walls and had diameter  $D=2$  m and depth  $L=0.1$  m while the flat plate PBR had height  $H=2$  m and thickness  $L=0.1$  m. In both cases, the initial mass concentration was  $X_0=0.1$  kg/m<sup>3</sup>.

the average total specific growth rate  $\bar{\mu}$  predicted based on  $G_\lambda(z)$  and  $G_{PAR}(z)$  predicted by the two-flux approximation fell within 1–7% of its numerically predicted value. These results suggest that

the two-flux approximation can be used to determine  $G_{PAR}(z)$  and the corresponding  $\bar{\mu}$  in open ponds or race ponds with dimensions larger than 2 m when shadow effects become less and less

significant. This can be very useful in the design and real time control and operation of open ponds.

Fig. 6b compares numerical results with predictions from the two-flux approximation [Eq. (18)] and the simplified two-flux approximation [Eq. (21)] for the PAR-averaged local fluence rate  $G_{PAR}(x)$  predicted at the centerline of the vertical flat-plate at 10:00 am, 2:00 pm, and 6:00 pm. The maximum relative difference between numerical results and predictions by the two-flux approximation for the local  $G_{PAR}(x)$  without refraction ranged between 4% and 22% while the relative differences averaged over the PBR volume were about 2–13% depending on the time of the day. The two-flux approximation tended to overpredict  $G_{PAR}(x)$  because it was not able to predict the shadow and other multi-dimensional effects. Moreover, the average total specific growth rate  $\bar{\mu}$  estimated using  $G_{PAR}(x)$  predicted by the two-flux approximation [Eq. (18)] fell within 2–10% of its numerically predicted values. Overall, the two-flux approximation predictions of  $G_{PAR}(x)$  and the corresponding average total specific growth rate  $\bar{\mu}$  in vertical flat-plate PBRs were acceptable. Finally, the average total specific growth rate  $\bar{\mu}$  in the vertical flat-plate PBR was found to be larger than that of an open pond of identical depth with black walls at all times except at 12:00 pm because the surface area exposed to sunlight was smaller.

#### 4.5. Comparison of daily areal biomass productivities

The daily areal biomass productivity of an open pond PBR, expressed in  $\text{kg/m}^2/\text{day}$ , was defined as the mass of microalgae produced after 12 h of exposure to sunlight per unit illuminated surface area exposed to collimated solar irradiance. It is expressed as

$$P_{op} = \frac{(X_f - X_0)V}{St_f} = \frac{(X_f - X_0)L}{t_f} = \frac{(X_f - X_0)}{a_{op}t_f} \quad (24)$$

where  $S$  and  $V$  are the illuminated surface area and volume of the PBR, respectively, while  $X_f$  is the final mass concentration and  $t_f$  is equal to 1 day. The specific illuminated area of the PBRs, denoted by  $a$  (in  $\text{m}^{-1}$ ), is defined as  $a = S/V$  (Cornet and Dussap, 2009). For an open pond of diameter  $D$ , thickness  $L$ , and illuminated surface area  $S = \pi D^2/4$ , the specific illuminated area is equal to  $a_{op} = 1/L$ . In addition, the initial optical thickness of open ponds is expressed as  $\beta_\lambda L = (\bar{A}_{abs,\lambda} + \bar{S}_{sca,\lambda})X_0L$  where the average mass cross-sections  $\bar{A}_{abs,\lambda}$  and  $\bar{S}_{sca,\lambda}$  are intrinsic properties of the microalgae species, respectively. Thus,  $X_0L = X_0a_{op}^{-1}$  can be considered as a representative of the PBR's initial optical thickness.

The daily areal biomass productivity per unit surface area exposed to collimated solar irradiance for vertical flat-plate and tubular PBRs, respectively, denoted by  $P_{fp}$  and  $P_{tb}$  (in  $\text{kg/m}^2/\text{day}$ ), are also defined in terms of specific illuminated area for flat-plate PBRs of thickness  $L$  ( $a_{fp} = HW/HWL = 1/L$ ) and for tubular PBRs of diameter  $L$  ( $a_{tb} = (\pi LW/2)/(\pi L^2W/4) = 2/L$ ). In other words,

$$P_{fp} = \frac{(X_f - X_0)L}{t_f} \quad \text{and} \quad P_{tb} = \frac{(X_f - X_0)L/2}{t_f} \quad (25)$$

here also  $X_f$  is the final concentration after a duration  $t_f$  of one day.

Fig. 7 shows the daily areal biomass productivity of open ponds  $P_{op}$ , vertical flat-plate  $P_{fp}$ , and tubular PBRs  $P_{tb}$  as a function of  $X_0a^{-1}$  for different values of their characteristics length  $L$  (i.e., depth, thickness, or diameter) varying from 0.05 to 1.0 m and initial concentration  $X_0$  between 0.1 and 5.0  $\text{kg/m}^3$ . The daily areal biomass productivity of vertical flat-plate  $P_{fp}$  was calculated based on  $\bar{\mu}$  estimated with  $G_{PAR}(x)$  predicted by the two-flux approximation, ignoring wall refraction. On the other hand,  $P_{tb}$  was calculated numerically based on  $G_{PAR}(\mathbf{r})$  and  $\bar{\mu}$ . It is interesting to note that the daily biomass productivities  $P_{op}$ ,  $P_{fp}$ , and  $P_{tb}$  depended uniquely on the product  $X_0a^{-1}$  and not on  $X_0$  and  $a$  or  $L$  independently.

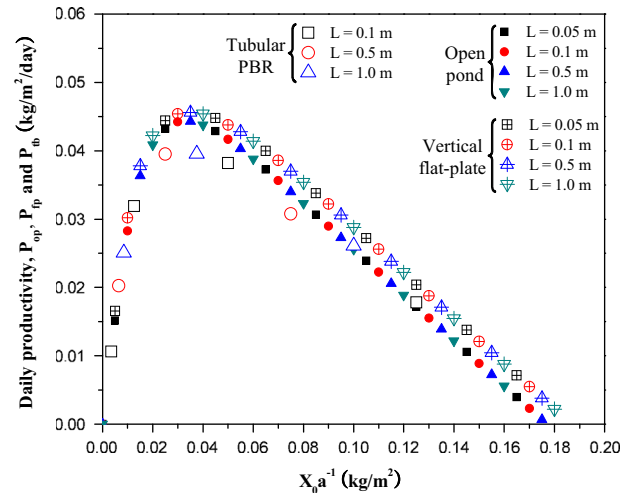


Fig. 7. Daily areal biomass productivity per unit illuminated surface area exposed to collimated solar irradiance predicted on June 21 in Los Angeles for open ponds  $P_{op}$ , vertical flat-plate PBRs  $P_{fp}$ , and tubular PBRs  $P_{tb}$  for *C. reinhardtii* as a function of  $X_0a^{-1}$  with depth or diameter  $L$  varying from 0.05 to 1.0 m and initial concentration  $X_0$  between 0.1 and 5.0  $\text{kg/m}^3$ . Here,  $a_{op} = 1/L$ ,  $a_{fp} = 1/L$ , and  $a_{tb} = 2/L$ .

Moreover, the productivities  $P_{op}$ ,  $P_{fp}$ ,  $P_{tb}$  versus  $X_0a^{-1}$  nearly overlapped regardless of the PBR geometry. The maximum daily areal productivity per unit illuminated surface area of these PBRs was  $P_{max} = 0.045 \text{ kg/m}^2/\text{day}$  for  $X_0a^{-1} = 0.035 \text{ kg/m}^2$ . For  $X_0a^{-1} < 0.035 \text{ kg/m}^2$ , the incident irradiance was not entirely absorbed by microalgae suspension as some photons were absorbed at the bottom of the open pond or transmitted through flat-plate or tubular PBRs. Then, the biomass productivity was low and increased with increasing optical thickness. However, for  $X_0a^{-1} > 0.035 \text{ kg/m}^2$ , dark region appeared in the PBRs thus decreasing the working illuminated volume while the effects of respiration became significant (Takache et al., 2012).

Note that the fact that the maximum productivity was identical for PBRs with the same specific illuminated area  $a$  irrespective of their geometry has already been predicted by Cornet and Dussap (2009) and experimentally validated by Takache et al. (2010). Here, we expanded this conclusion by demonstrating that the productivities per unit of illuminated surface area of PBRs are identical (including at their maximum) as long as they feature the same value of optical thickness represented by  $X_0a^{-1}$ . These results should be evaluated in combination with the associated capital and operational costs (Chaumont, 1993). The same design tool could also be used to investigate shading between cultivation systems but this effort falls outside the scope of the present study.

Finally, the fact that daily biomass productivities  $P_{op}$ ,  $P_{fp}$ , and  $P_{tb}$  depend only on the product  $X_0a^{-1}$  provides a simple and practical way to design (via  $a$ ) and to operate (via  $X_0$ ) these PBRs to achieve maximum productivity in batch mode. Indeed, to achieve the maximum daily production rate from the specific microalgae grown in any of the three PBRs considered, one should geometrically design the PBRs specific illuminated surface area and set the initial concentration  $X_0$  so that  $X_0a^{-1} = 0.035 \text{ kg/m}^2$ . However, one may wonder if these results are valid for (i) other types of PBRs, (ii) for continuous operation, (iii) for different light transfer and growth kinetic models, and if they are supported by experimental evidences.

#### 4.6. Comparison with experimental data and other models

Pruvost et al. (2011) cultivated *Neochloris oleoabundans* in vertical flat-plate air-lift PBRs operated in continuous mode with different

thicknesses  $L=0.03$  and  $0.055$  m. The authors also modeled the process using the two-flux approximation to calculate the fluence rate in the PBRs. The growth kinetics model ignored photoinhibition but accounted for respiration and for the effect of dilution to predict the volumetric and areal productivities. The parameters  $\mu_0$ ,  $K_S$ , and  $\mu_s$  were estimated from experimental data as  $0.21 \text{ h}^{-1}$ ,  $90 \mu\text{mol photon m}^{-2} \text{ s}^{-1}$ , and  $0.005 \text{ h}^{-1}$ , respectively. Fig. 8a shows the experimentally measured and predicted daily areal biomass productivity of vertical flat-plate air-lift PBRs reported by Pruvost et al. (2011). First, it indicates that the productivity measured experimentally had the same order of magnitude as those reported in Fig. 7. Fig. 8a also establishes that the areal productivity of continuous air-lift PBRs was also a unique function of  $X_0 a^{-1}$ . Note that finding additional experimental data to further validate our results was made difficult by the fact that experimentally the PBR geometry and size as well as the initial concentration are arbitrarily set. Indeed, experimental parametric study similar to that performed

numerically in the present study would be very time consuming and potentially costly.

Moreover, Fig. 8b shows the simulation results reported by Slegers et al. (2011) for yearly volumetric biomass production (in  $\text{kg/m}^3/\text{year}$ ) for vertical flat-plate PBRs operated in continuous mode with *P. tricornutum* and *T. pseudonana*. Here, the PBR thickness ranged from  $0.05$  to  $0.1$  m and concentrations varied between  $1.0$  and  $13.0 \text{ kg/m}^3$ . It is very interesting to observe that these data obtained independently using different light and kinetics models collapsed also on a single line when plotted as a function of  $X_0 a^{-1}$ , whereas they were scattered when plotted as a function of  $L = 1/a$  (Fig. 3 in the manuscript by Slegers et al., 2011). Note also that this was not observed when defining the productivity per unit surface of ground footprint and per unit volume of PBR (see Supplementary Material). This may be attributed to the fact that the illuminated surface area is closely related to the solar energy input entering the PBR. In other words, the amount of biomass produced remains the same regardless of the PBR geometry for a given amount of solar energy absorbed.

## 5. Conclusion

This study presented accurate 3D numerical simulations for coupled light transfer and growth kinetics in the most commonly used PBRs exposed to collimated and diffuse sunlight in Los Angeles on June 21. The local fluence rate was predicted on a spectral basis by solving the 3D RTE. The temporal evolution of microalgae mass concentration was predicted by accounting for light saturation, photolimitation, and respiration. In open ponds, the reflecting walls resulted in a more uniform light distribution and increased the local fluence rate. However, the difference in overall biomass concentration after 12 h was negligible. Similarly, refraction by the container walls, in vertical flat-plate PBRs, had no significant effect on the microalgae concentration. The study demonstrated that the two-flux approximation can be used to estimate the local fluence rate in open (or race) ponds and flat-plate PBRs for all practical purposes including designing, controlling, and operating PBRs. Finally, the daily areal biomass productivity per unit illuminated surface area was found to depend uniquely on the initial optical thickness represented by  $X_0 a^{-1}$  for open ponds and tubular PBRs operated in batch mode. Similar results were obtained for the daily productivity per unit surface area illuminated for flat-plate PBRs. Moreover, the same conclusions were drawn by revisiting both experimental data and numerical simulations reported in the literature for similar and other PBR types cultivating other microorganisms in continuous mode. The parameter  $X_0 a^{-1}$  is useful and simple for designing (via  $a$ ) and operating (via  $X_0$ ) these PBRs at their maximum productivity.

## Nomenclature

$I$	radiation intensity, $\text{W/m}^2 \text{ sr}$
$\mathbf{r}$	position vector, m
$\hat{\mathbf{s}}$	direction unit vector
$G$	fluence rate, $\text{W/m}^2$
$\bar{A}_{abs}$	average mass absorption cross-section, $\text{m}^2/\text{kg}$
$\bar{S}_{sca}$	average mass scattering cross-section, $\text{m}^2/\text{kg}$
$X$	microorganism mass concentration, $\text{kg/m}^3$
$b$	backward scattering fraction
$t$	time, h
$K_S$	light half-saturation constant, $\mu\text{mol photon m}^{-2} \text{ s}^{-1}$
$K_I$	light inhibition constant, $\mu\text{mol photon m}^{-2} \text{ s}^{-1}$
$V$	volume, $\text{m}^3$
$S$	surface area, $\text{m}^2$
$H$	height, m

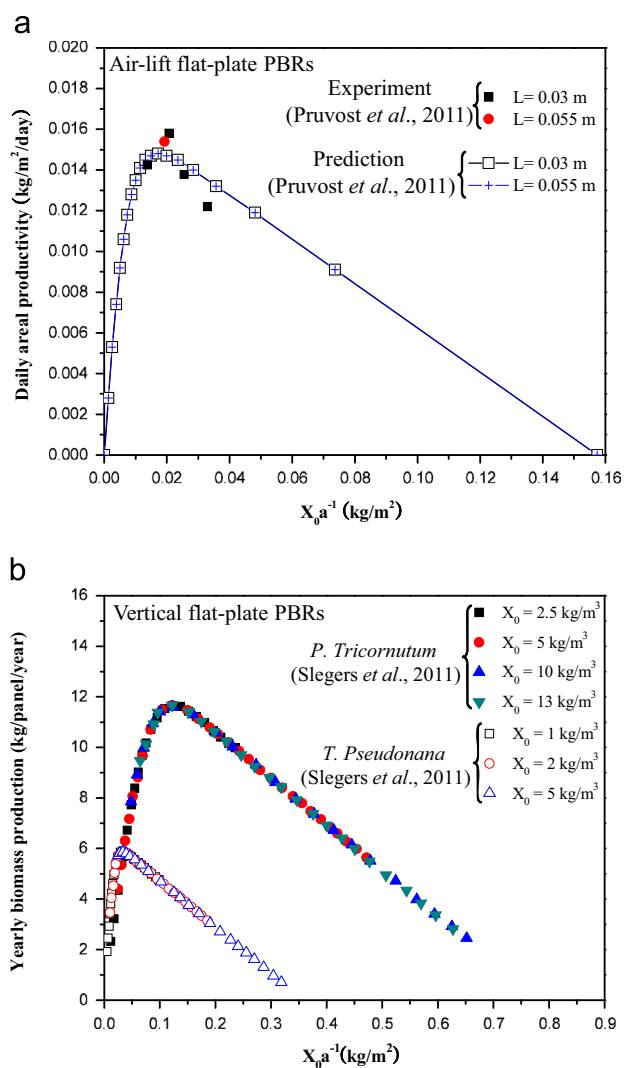


**Fig. 8.** (a) Experimentally measured and predicted daily areal biomass productivity as a function of  $X_0 a^{-1}$  for continuous vertical air-lift flat-plate PBR of thickness  $L$  equals to 3 or 5.5 cm with *N. oleoabundans* (Pruvost et al., 2011). (b) Collapse of the predicted yearly volumetric biomass productivity shown in Fig. 3 in Slegers et al. (2011) plotted as a function of  $X_0 a^{-1}$  for 1 m tall vertical flat-plate PBRs in continuous operation with  $L$  varying from 0.05 to 0.1 m and  $X_0$  between 1.0 and  $13.0 \text{ kg/m}^3$  for *P. tricornutum* and *T. pseudonana*.

$W$	width, m
$L$	thickness, m
$D$	diameter, m
$n$	refractive index
$P$	daily areal biomass productivity, kg/m <sup>2</sup> /day
$a$	specific illuminated area, m <sup>-1</sup>

## Greek symbols

$\kappa$	absorption coefficient, m <sup>-1</sup>
$\sigma_s$	scattering coefficient, m <sup>-1</sup>
$\beta$	extinction coefficient, m <sup>-1</sup>
$\Phi$	scattering phase function
$\Omega$	solid angle, sr
$\theta, \phi$	spherical coordinate
$\bar{\mu}$	average total specific growth rate, h <sup>-1</sup>
$\mu_p$	photosynthetic specific growth rate, h <sup>-1</sup>
$\mu_0$	maximum specific growth rate, h <sup>-1</sup>
$\mu_s$	respiration rate, h <sup>-1</sup>
$\mu$	local specific growth rate, h <sup>-1</sup>

## Subscripts

$\lambda$	wavelength
PAR	average over the photosynthetically active region
av	average over the photobioreactor
$c$	collimated
$d$	diffuse
0	initial
$f$	final
op	open pond
fp	vertical flat-plate photobioreactor
tb	tubular photobioreactor
max	maximum

## Appendix A. Supplementary data

Supplementary data associated with this article can be found in the online version at <http://dx.doi.org/10.1016/j.ces.2013.11.014>.

## References

- Aiba, S., 1982. Growth kinetics of photosynthetic microorganisms. *Adv. Biochem. Eng./Biotechnol.* 23, 85–156.
- Asenjo, J., Merchuk, J., 1995. *Bioreactor System Design*. Marcel Dekker, New York, NY.
- Barsanti, L., Gualtieri, P., 2005. *Algae: Anatomy, Biochemistry, and Biotechnology*. CRC Press, Boca Raton, FL.
- Berberoglu, H., Pilon, L., 2007. Experimental measurement of the radiation characteristics of *Anabaena variabilis* ATCC 29413-U and *Rhodospira rubra* ATCC 49419. *Int. J. Hydrog. Energy* 32 (18), 4772–4785.
- Berberoglu, H., Pilon, L., 2010. Maximizing solar to H<sub>2</sub> energy conversion efficiency of outdoor photobioreactors using mixed cultures. *Int. J. Hydrog. Energy* 35, 500–510.
- Berberoglu, H., Yin, J., Pilon, L., 2007a. Light transfer in bubble sparged photobioreactors for H<sub>2</sub> production and CO<sub>2</sub> mitigation. *Int. J. Hydrog. Energy* 32, 2273–2285.
- Berberoglu, H., Yin, J., Pilon, L., 2007b. Simulating light transfer in a bubble sparged photobioreactor for simultaneous hydrogen fuel production and CO<sub>2</sub> mitigation. *Int. J. Hydrog. Energy* 32 (13), 2273–2285.
- Berberoglu, H., Melis, A., Pilon, L., 2008. Radiation characteristics of *Chlamydomonas reinhardtii* C125 and its truncated chlorophyll antenna transformants *tla1*, *tlaX*, and *tla1-CW+*. *Int. J. Hydrog. Energy* 33 (22), 6467–6483.
- Chaumont, D., 1993. Biotechnology of algal biomass production: a review of systems for outdoor mass culture. *J. Appl. Phycol.* 5, 593–604.
- Chisti, Y., 2007. Biodiesel from algae. *Biotechnol. Adv.* 25, 294–306.
- Chui, E., Raithby, G., 1993. Computation of radiant-heat transfer on a nonorthogonal mesh using the finite-volume method. *Numer. Heat Transf. Part B—Fund.* 23 (3), 269–288.
- Cornet, J., Albiol, J., 2000. Modeling photoheterotrophic growth kinetics of *Rhodospirillum rubrum* in rectangular photobioreactors. *Biotechnol. Prog.* 16, 199–207.
- Cornet, J., Dussap, C., 2009. A simple and reliable formula for assessment of maximum volumetric productivities in photobioreactors. *Biotechnol. Prog.* 25, 424–435.
- Cornet, J.-F., Dussap, C., Dubertret, G., 1992. A structured model for simulation of cultures of the cyanobacterium *Spirulina platensis* in photobioreactors: I. Coupling between light transfer and growth kinetics. *Biotechnol. Bioeng.* 40 (7), 817–825.
- Dunn, I., Heinze, E., Ingham, J., Prenosil, J., 2003. *Biological Reaction Engineering: Dynamic Modelling Fundamentals with Simulation Examples*, 2nd ed. Wiley-VCH.
- Fiveland, W., Wessel, R., 1988. Numerical model for predicting performance of three-dimensional pulverized-fuel fired furnaces. *ASME J. Eng. Gas Turbines Power* 110 (1), 117–126.
- Fouchard, S., Pruvost, J., Degrenne, B., Titica, M., Legrand, J., 2009. Kinetic modeling of light limitation and sulfur deprivation effects in the induction of hydrogen production with *Chlamydomonas reinhardtii*: Part I. Model development and parameter identification. *Biotechnol. Bioeng.* 102 (1), 232–245.
- Geider, R., MacIntyre, H., Kana, T., 1996. A dynamic model of photoadaptation in phytoplankton. *Limnol. Oceanogr.* 41, 1–15.
- Gueymard, C., 2002. SMARTS Code, Version 2.9.2 User's direct beam spectral irradiance data for photovoltaic cell Manual. Solar Consulting Services, (<http://rredc.nrel.gov/solar/models/SMARTS>).
- Hale, G., Query, M., 1973. Optical constants of water in the 200-nm to 200- $\mu$ m wavelength region. *Appl. Opt.* 12, 555–563.
- He, X., Lee, E., Wilcox, L., Muniipalli, R., Pilon, L., 2013. A high-order accurate GPU-based radiative transfer equation solver for combustion and propulsion applications. *Numer. Heat Transfer Part B—Fund.* 63 (6), 457–484.
- Huang, Q., Yao, L., Liu, T., Yang, J., 2012. Simulation of the light evolution in an annular photobioreactor for the cultivation of *Porphyridium cruentum*. *Chem. Eng. Sci.* 84, 718–726.
- Janssen, M., Bresser, L.D., Baijens, T., Tramper, J., Mur, L., Snel, J., Wijffels, R., 2000. Scale-up aspects of photobioreactors: effects of mixing-induced light/dark cycles. *J. Appl. Phycol.* 12, 225–237.
- Le Borgne, F., Pruvost, J., 2013. Investigation and modeling of biomass decay rate in the dark and its potential influence on net productivity of solar photobioreactors for microalga *Chlamydomonas reinhardtii* and cyanobacterium *Arthrospira platensis*. *Bioresour. Technol.* 138, 271–276.
- Lee, E., Heng, R.-L., Pilon, L., 2013. Spectral optical properties of selected photosynthetic microalgae producing biofuels. *J. Quant. Spectrosc. Radiat. Transfer* 114, 122–135.
- Li, H.-S., Flamant, G., Lu, J.-D., 2004. A new discrete ordinate algorithm for computing radiative transfer in one-dimensional atmospheres. *J. Quant. Spectrosc. Radiat. Transfer* 83, 407–421.
- Melis, A., 2002. Green alga hydrogen production: process, challenges and prospects. *Int. J. Hydrog. Energy* 27 (11–12), 1217–1228.
- Modest, M., 2003. *Radiative Heat Transfer*. Academic Press, San Diego, CA.
- Morel, A., Smith, R., 1974. Relation between total quanta and total energy for aquatic photosynthesis. *Limnol. Oceanogr.* 19, 591–600.
- Morweiser, M., Kruse, O., Hankamer, B., Posten, C., 2010. Developments and perspectives of photobioreactors for biofuel production. *Appl. Microbiol. Biotechnol.* 87, 1291–1301.
- Muller-Feuga, A., Guédes, R.L., Pruvost, J., 2003. Benefits and limitations of modeling for optimization of *Porphyridium cruentum* cultures in an annular photobioreactor. *J. Biotechnol.* 103, 153–163.
- Murphy, T., Berberoglu, H., 2011. Effect of algae pigmentation on photobioreactor productivity and scale-up: a light transfer perspective. *J. Quant. Spectrosc. Radiat. Transfer* 112, 2826–2834.
- Pilon, L., Berberoglu, H., Kandilian, R., 2011. Radiation transfer in photobiological carbon dioxide fixation and fuel production by microalgae. *J. Quant. Spectrosc. Radiat. Transfer* 112 (17), 2639–2660.
- Posten, C., 2009. Design principles of photo-bioreactors for cultivation of microalgae. *Eng. Life Sci.* 9, 165–177.
- Pottier, L., Pruvost, J., Deremetz, J., Cornet, J.-F., Legrand, J., Dussap, C., 2005. A fully predictive model for one-dimensional light attenuation by *Chlamydomonas reinhardtii* in a torus photobioreactor. *Biotechnol. Bioeng.* 91, 569–582.
- Pruvost, J., Vooren, G.V., Guic, B.L., Couzinet-Mosson, A., Legrand, J., 2011. Systematic investigation of biomass and lipid productivity by microalgae in photobioreactors for biodiesel application. *Bioresour. Technol.* 102, 150–158.
- Pruvost, J., Cornet, J.F., Goetz, V., Legrand, J., 2012. Theoretical investigation of biomass productivities achievable in solar rectangular photobioreactors for the cyanobacterium *Arthrospira platensis*. *Biotechnol. Prog.* 28, 699–714.
- Richmond, A., 1996. Efficient utilization of high irradiance for production of photoautotrophic cell mass: a survey. *J. Appl. Phycol.* 8 (4–5), 381–387.
- Richmond, A., 2004. Principles for attaining maximal microalgal productivity in photobioreactors: an overview. *Hydrobiologia* 512 (1–3), 33–37.
- Richmond, A., Qiang, H., 1997. Principles for efficient utilization of light for mass production of photoautotrophic microorganisms. *Appl. Biochem. Biotechnol.* 63–65 (1), 649–658.
- Skjånes, K., Lindblad, P., Muller, J., 2007. BioCO<sub>2</sub>—a multidisciplinary, biological approach using solar energy to capture CO<sub>2</sub> while producing H<sub>2</sub> and high value products. *Biomol. Eng.* 24 (4), 405–413.
- Slegers, P., Wijffels, R., van Straten, G., van Boxtel, A., 2011. Design scenarios for flat panel photobioreactors. *Appl. Energy* 88, 3342–3353.
- Takache, H., Christophe, G., Cornet, J.-F., Pruvost, J., 2010. Experimental and theoretical assessment of maximum productivities for the microalga *Chlamydomonas reinhardtii* in two different geometries of photobioreactors. *Biotechnol. Prog.* 26, 431–440.
- Takache, H., Pruvost, J., Cornet, J.-F., 2012. Kinetic modeling of the photosynthetic growth of *Chlamydomonas reinhardtii* in a photobioreactor. *Biotechnol. Prog.* 28 (3), 681–692.
- Ugwu, C., Aoyagi, H., Uchiyama, H., 2008. Photobioreactors for mass cultivation of algae. *Bioresour. Technol.* 99, 4021–4028.

Versyck, K., Claes, J., Impe, J.V., 1997. Practical identification of unstructured growth kinetics by application of optimal experimental design. *Biotechnol. Prog.* 13 (5), 524–531.

Wheaton, Z., Krishnamoorthy, G., 2012. Modeling radiative transfer in photobioreactors for algal growth. *Comput. Electr. Agric.* 87, 64–73.

Yoon, J., Sim, S., Kim, M., Park, T., 2002. High cell density culture of *Anabaena variabilis* using repeated injections of carbon dioxide for the production of hydrogen. *Int. J. Hydrog. Energy* 27 (11–12), 1265–1270.